Multiple Exciton Generation in Colloidal Silicon Nanocrystals

Matthew C. Beard,*,† Kelly P. Knutsen,† Pingrong Yu,†,‡ Joseph M. Luther,†,§ Qing Song,† Wyatt K. Metzger,† Randy J. Ellingson,*,† and Arthur J. Nozik*,†,∥

National Renewable Energy Laboratory, Golden, Colorado 80401, Innovalight, Inc., Santa Clara, California 95054, Department of Applied Physics, Colorado School of Mines, Golden, Colorado 80401, and Department of Chemistry, University of Colorado, Boulder, Colorado 80309

Received June 22, 2007

ABSTRACT

Multiple exciton generation (MEG) is a process whereby multiple electron–hole pairs, or excitons, are produced upon absorption of a single photon in semiconductor nanocrystals (NCs) and represents a promising route to increased solar conversion efficiencies in single-junction photovoltaic cells. We report for the first time MEG yields in colloidal Si NCs using ultrafast transient absorption spectroscopy. We find the threshold photon energy for MEG in 9.5 nm diameter Si NCs (effective band gap ≡ E_g = 1.20 eV) to be 2.4 ± 0.1E_g and find an exciton-production quantum yield of 2.6 ± 0.2 excitons per absorbed photon at 3.4E_g. While MEG has been previously reported in direct-gap semiconductor NCs of PbSe, PbS, PbTe, CdSe, and InAs, this represents the first report of MEG within indirect-gap semiconductor NCs. Furthermore, MEG is found in relatively large Si NCs (diameter equal to about twice the Bohr radius) such that the confinement energy is not large enough to produce a large blue-shift of the band gap (only 80 meV), but the Coulomb interaction is sufficiently enhanced to produce efficient MEG. Our findings are of particular importance because Si dominates the photovoltaic solar cell industry, presents no problems regarding abundance and accessibility within the Earth's crust, and poses no significant environmental problems regarding toxicity.

Silicon semiconductor technology not only stands as the foundation of today's widely manufactured integrated circuit technology but also comprises more than 90% of all photovoltaic (PV) cell production. The Shockley–Queisser detailed balance power conversion efficiency limit for a typical single-junction crystalline silicon PV cell under the standard AM1.5 solar spectrum is ∼33%. The 67% of incident solar power not converted to electrical power includes: ∼47% converted to heat through phonon emission caused by inelastic scattering of hot electrons and holes with the crystal lattice subsequent to absorption of supraband gap photons, ∼18.5% lost to transmission of sub-band gap photons, and ∼1.5% lost through radiative recombination. The prevention of hot carrier cooling via phonon emission may ultimately yield meaningful efficiency gains for solar photon conversion.[1,2] Efficient generation of multiple excitons per absorbed photon of energy greater than twice the band gap represents one possible route toward enhanced photon conversion efficiency. In bulk semiconductors, a related process can create multiple free electrons and holes (charge carriers) by a process called impact ionization. In

semiconductor nanocrystals (NCs), we believe a new mechanism that represents new photophysics is needed to explain MEG. First, excitons (bound electron–hole pairs), not free carriers, are initially produced in NCs. Second, in NCs, the requirement for the conservation of crystal momentum is relaxed (i.e., **k** is not a good quantum number);[3–5] this results in a lower threshold photon energy for electron–hole pair multiplication processes because only energy must be conserved. Third, the process of MEG has been shown to occur with significantly higher efficiencies in PbSe, PbS, PbTe, CdSe, and InAs NCs[6–11] compared to that of impact ionization (carrier multiplication) in bulk semiconductors. Finally, MEG occurs at very high rates, much faster than competing relaxation channels such as hot electron–hole pair cooling or Auger recombination of multiple electron–hole pairs (the reverse process of MEG). For these reasons, we prefer the term MEG rather than carrier multiplication; the latter cannot occur until the excitons are dissociated into free, separated electrons and holes. We explain the novel process of MEG via a quantum mechanical model that invokes a coherent superposition of multiple excitonic states.[8,12]

Here, we report for the first time efficient MEG in Si NCs measured by transient absorption spectroscopy and find that the threshold photon energy for MEG is 2.4 ± 0.1E_g and that the quantum yield (QY) of excitons produced per absorbed photon reaches 2.6 ± 0.2 at 3.4E_g. In contrast, for

* To whom correspondence should be addressed. E-mail: matt_beard@nrel.gov (M.C.B.); randy_ellingson@nrel.gov (R.J.E.); anozik@nrel.gov (A.J.N.).
† National Renewable Energy Laboratory.
‡ Innovalight, Inc..
§ Department of Applied Physics, Colorado School of Mines.
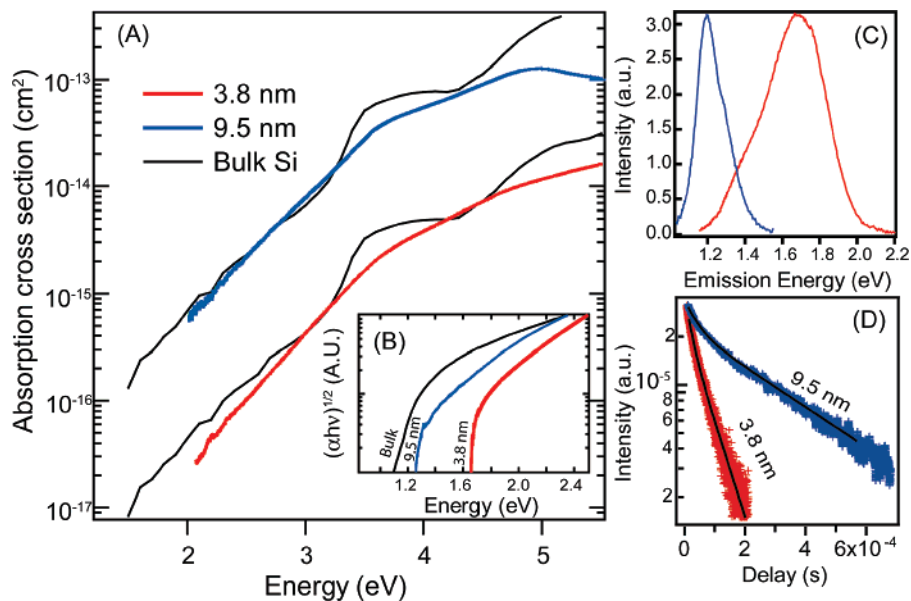∥ Department of Chemistry, University of Colorado.

Figure 1. Linear optical properties of colloidal Si NCs studied in this report. (A) The absorption cross section for the NCs dispersed in hexane. Black lines show the computed cross section of the NCs based on an equivalent bulk Si volume. Part (B) displays the onset of the absorption in a Tauc plot showing the blue-shifted absorption onset. (C) PL spectra. (D) PL lifetime data measured at the peak of the emission wavelength (red line 3.8 nm, blue line 9.5 nm). The peak of the emission spectrum is taken as the effective band gap for each of the NC samples, yielding bandgaps of 1.68 eV for the 3.8 nm NCs and 1.20 eV for the 9.5 nm NCs.

bulk Si, the threshold for impact ionization is ~$3.5E_g$ and the QY rises to only ~1.4 at $4.5E_g$.[13] Because there are very few solar photons above $3.5E_g$, impact ionization in bulk Si is not a useful approach for enhancing PV efficiencies. However, highly efficient MEG in nanocrystalline Si at lower photon energies in the visible region has the potential to increase power conversion efficiency in Si-based PV cells toward a thermodynamic limit of ~44% at standard AM1.5 solar intensity; it also could result in efficient direct photolytic decomposition of water for hydrogen production.[2]

Colloidal Si NC samples (Innovalight, Inc.), having average diameters of 9.5 and 3.8 nm with size distributions of 15%, were dispersed in either tetrachloroethylene or hexane. The preparation of the Si NC samples has been described previously.[14] The optical properties of Si NCs differ significantly from those of bulk Si. Figure 1A displays the measured absorption cross sections and compares them to values calculated from an equivalent volume of bulk Si,[15] accounting for the dielectric screening of the solvent. The absorption onset (Figure 1B) shows a strong size-dependent blue-shift, and the NCs exhibit relatively strong photoluminescence (Figure 1C). Silicon NCs with well-passivated surfaces yield exciton lifetimes extending to hundreds of microseconds, reflecting defect-free, indirect-gap NCs (Figure 1D), with high photoluminescence (PL) efficiencies (>50%) in the absence of oxygen.[16,17] No discernible excitonic transition is observed because, for the sizes studied here, Si remains an indirect-gap semiconductor.[18] Apart from the blue-shift of the effective band gap, the linear light absorption properties of colloidal Si NCs closely mimic that of bulk Si, with substantially broadened features that correspond to the direct Γ−Γ and L−L transitions. We assume no Stokes shift in accord with previous observations[18,19] and associate the effective NC band gap with the

peak of the PL spectrum: 1.20 and 1.68 eV for Si NC diameters of 9.5 and 3.8 nm, respectively (see Figure 1C). We observe biexponential PL decay times,[5] which increase with NC diameter: the longest time constant increases from 72 ± 2 μs for 3.8 nm NCs to 350 ± 10 μs for 9.5 nm NCs (Figure 1D).

To study MEG, we employ femtosecond transient absorption (TA) spectroscopy. In general, TA can probe the exciton population dynamics in NCs by monitoring either an interband absorption bleach associated with population state-filling or an intraband photoinduced absorption (PA) associated with transitions within the conduction or valence band.[8] Silicon's indirect band structure yields extremely weak linear absorption at the band gap, and thus one cannot readily probe a state-filling-induced bleach. Instead, we probe the exciton population dynamics by photoinduced intraband absorption changes. Figure 2A displays the PA spectrum as a function of the probe photon energy; a free-carrier model with $1/\omega^2$ dependence fits the data well. We do not observe any absorbance for energies less than ~0.95 eV in the absence of the pump laser. For the majority of the experiments, we probe at 0.86 eV, well below the effective band gap. We verified that the photoinduced dynamics do not depend on the probe energy over a broad range from 0.28 to ~2 eV. All measurements were performed at room temperature.

The ability to quantitatively characterize the quantized N-exciton decay dynamics is the key to identifying MEG in semiconductor NCs.[7,20] Photoexcitation creates a highly excited exciton in the NC that may follow several competing relaxation pathways (see Figure 2B) to reach the lowest excited 1S state. For efficient multiexciton formation, the rate of MEG must be large compared to all competing processes. However, as of yet, this rate has not been
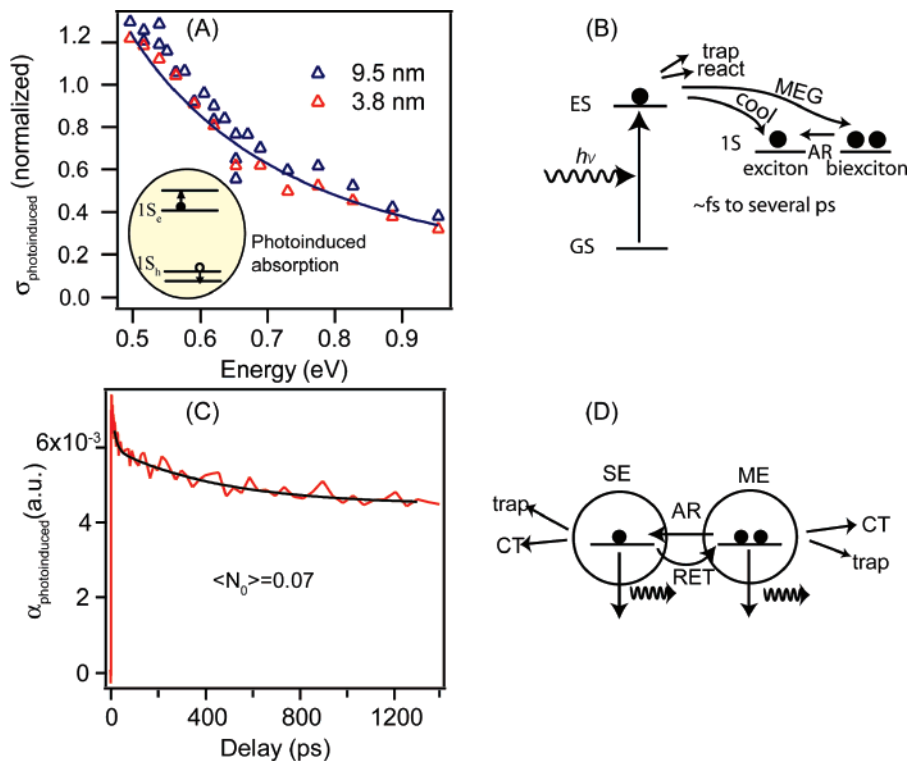
Figure 2. (A) Normalized photoinduced absorption cross section as a function of probe photon energy for two different sizes of NCs (3.8 nm red triangles, and 9.5 nm blue triangles). The pump wavelength was 600 nm with 3.4×10^{15} photons cm^{-2} s^{-1} fluence and the probe delay was 10 ps. (B) Photoexcitation of the ground state (GS) of a NC produces an exciton in a highly excited state (ES). The "hot" exciton may undergo several different relaxation pathways such as trapping, photoreaction, hot exciton cooling, or MEG. (C) Low excitation intensity photoinduced absorption dynamics for 9.5 nm diameter sample, showing the intrinsic single-exciton decay dynamics (D) Possible relaxation channels for single- (SE) and multiexciton (ME) states. Both the SE and ME state may undergo trapping or charge transfer (CT). The ME state can undergo Auger recombination (AR) to become a SE ,while the SE may undergo resonant energy transfer (RET) to become a ME.

measured directly in Si NCs from rise time data. Multiexciton production therefore is determined by analyzing the decay data in the ps to ns time regime.

When exciting a colloidal solution of NCs using a laser pulse width that is short compared to exciton recombination dynamics, the average number of photons absorbed per NC, $\langle N_0 \rangle$, can be calculated by the product of the absorption cross section, σ_a, and the pump photon fluence, j_p: $\langle N_0 \rangle = \sigma_a \cdot j_p$. The number of NCs that have absorbed m photons can be determined by the Poisson distribution function; $n_m = n_{NC}P(m)$, where $P(m) = \langle N_0 \rangle^m \exp(-\langle N_0 \rangle)/m!$ and n_{NC} is the concentration of NCs in the photoexcitation volume. Figure 2C shows the measured PA decay dynamics for 9.5 nm sample photoexciting at 2.07 eV ($1.7E_g$) with $\langle N_0 \rangle = 0.07$ and therefore represents the intrinsic single exciton decay dynamics (under these conditions, only ~3% of the excited NCs absorb more than one photon per NC).

Independent of NC size, each of the samples we have studied exhibits a similar, apparently intrinsic, multiexponential single-exciton decay whose shape remains independent of pump wavelength below the MEG threshold. The single-exciton state for these samples decays multiexponentially, suggestive of surface-mediated recombination or trapping processes. An ensemble of Si NCs exhibits electronic behavior indicative of a polydisperse sample due to some NCs containing efficient nonradiative defects, varying surface quality, or shape variation. As shown in Figure 1D,

single-exciton lifetimes fall in the range of 10^{-5} to 10^{-4} s for Si NCs 4–10 nm in diameter. Figure 2D is a schematic showing the possible relaxation channels for single-exciton (SE) and multiexciton (ME) states. Single-exciton states may undergo processes such as surface trapping, charge transfer (CT), which may involve trapping of the electron or hole at the surface, and radiative recombination. However, when two or more excitons occupy a NC (for a 3.8 nm diameter NC, two excitons corresponds to a volume carrier density exceeding 10^{19} cm^{-3}), Auger recombination (AR) on the 10^{-10} to 10^{-11} s time scale dominates the exciton decay process until each photoexcited NC contains one exciton. Figure 3A shows the intensity dependence of the PA signal dynamics under the same conditions as noted for Figure 2C. The value of $\langle N_0 \rangle$ for these data varies from 0.07 to 1.5. As $\langle N_0 \rangle$ increases, a new decay channel emerges. All of these traces in Figure 3A may be simultaneously modeled within a global fitting routine using only two adjustable parameters, the AR rate (or biexciton lifetime), and the absorption cross section at the pump wavelength.[8] The smooth black lines in Figure 3A are the results of the fit with $t_2 = 500 \ (\pm 20)$ ps and $\sigma_p = 4.0 \ (\pm .2) \times 10^{-16}$ cm^2. Figure 3B, which includes the biexciton lifetime value we measured for a 6.8 nm Si NC sample, shows that the biexciton decay times for three different Si NC sizes depend linearly on the NC volume, in
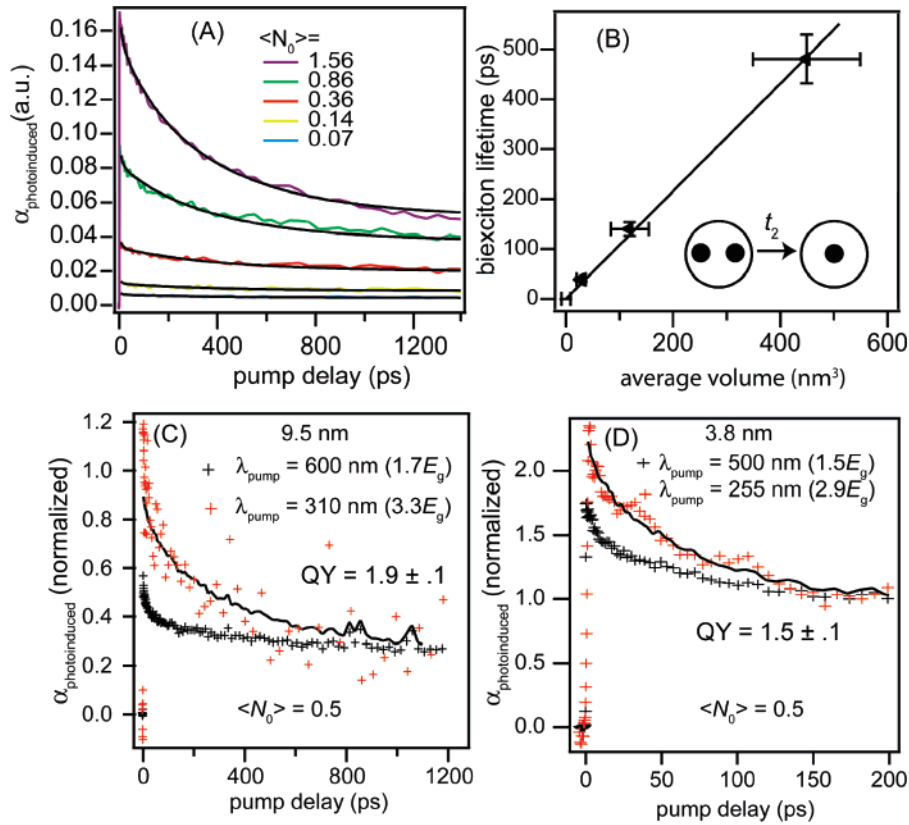
Figure 3. (A) Intensity-dependent exciton population decay dynamics for 9.5 nm diameter sample. The increasing amplitude of the 500 ps decay component reflects biexciton decay through Auger recombination. (B) Size dependence of the extracted biexciton decay times for three Si NC sizes. The biexciton lifetime, τ_2, scales linearly with NC volume. Note that the error in the biexciton lifetimes are not as large as the size distribution. (C) Transient absorption of 9.5 nm Si NCs photoexciting above and below the MEG threshold for a fixed excitation level of $\langle N_o \rangle = 0.5$. The black line is a fit to the above-MEG threshold data (see text). (D) Same as (C) except for the 3.8 nm sample.

agreement with the AR mechanism.[20] Thus the new decay channel at high pump fluences is assigned to nonradiative AR.

When photoexciting above the energy conservation threshold for MEG ($>2E_g$) at low intensity, so that each photoexcited NC absorbs at most one photon, multiexciton AR serves as a metric for MEG. The amplitude of the AR component increases as the photon energy increases past the energy threshold for efficient MEG to occur. Parts C and D of Figure 3 indicate the decay dynamics when $\langle N_0 \rangle$ is held constant at 0.5 at different pump wavelengths for the 9.5 and 3.8 nm samples, respectively. The black crosses are the decay dynamics for pump energies of 1.7 and $1.5E_g$ (below the MEG threshold), and the red crosses are for photon energies of 3.3 and $2.9E_g$ (above the MEG threshold). The data at long times (>300 ps) in Figure 3C for the $3.3E_g$ pump are noisy, but the presence of the new fast decay component at times <300 ps is clearly evident. We model our data with only one adjustable parameter: the MEG efficiency, η. The fitting function has the following form:

$$\alpha(t; h\nu_{pump} > 2E_g) = \alpha(t; h\nu_{pump} < 2E_g)$$

$$+ \sum_{k=2}^{\infty} a_k'(\eta) \exp(-\tau/t_k) \quad (1)$$

where $a_k'(\eta)$ are the contributions to the bi ($k = 2$), tri ($k = 3$), etc., populations that arise from MEG. The $a_k'(\eta)$ depend upon whether MEG is able to produce 1, 2, 3, etc., additional excitons per absorbed photon.[8] We reproduce $a_k'(\eta)$ for $3E_g < h\nu < 4E_g$, where MEG may produce 1 or 2 additional excitons per absorbed photon.

$$a_k'(\eta) = \sum_{m=\left\lceil \frac{k}{3} \right\rceil}^{k-1} P(m) \sum_{j=k-l}^{2m} \eta^j(1-\eta)^{2m-j} \frac{(2m)!}{(2m-j)!j!}$$

$$(3E_g < h\nu < 4E_g) \quad (2)$$

where $P(m)$ is the Poisson distribution. The t_k in eq 1 follow from the biexciton lifetime: $t_k = 4t_2/k^2$.[20] The $a_k'(\eta)$ are determined by $\langle N_0 \rangle$, which is an experimentally determined parameter, and η. In the fit, η is the only adjustable parameter and is related to the QY either by QY $= \eta + 1$ for $2E_g < h\nu < 3E_g$ and QY $= 2\eta + 1$ for $3E_g < h\nu < 4E_g$. We find that, for Figure 3C, the QY is 1.9 ± 0.1, and for Figure 3D, the QY is 1.5 ± 0.2.

By photoexciting above the energy conservation threshold for MEG ($>2E_g$) and at low intensity so that each photoexcited NC absorbs at most one photon, the appearance in Figure 3 of fast multiexciton Auger recombination serves

as a signature for MEG. We have ruled out other processes as possible sources of this decay component. As an example, one might consider resonant energy transfer (RET) of an exciton from one NC to another NC, which already has an exciton as a way to produce a single- to multiexciton transition, thereby creating multiexcitons per absorbed photon. However, the rate of RET would decrease at low photon fluences, in contrast to what is observed. For nanocrystals, the distance scale is so small that recombination at surface states should not depend on generation depth and hence excitation wavelength as observed here. Surface recombination into a continuum of high energy states would need to be much faster than the dynamics observed here to compete with carrier cooling. Similarly, fast transient absorption from impurities excitable only at high photon energies would not show a steady amplitude increase with decreasing excitation wavelength, as observed here. We cannot envision any alternative process other than MEG that is consistent with the following experimentally determined observations: (1) the dynamics are the same as AR (same decay rate and dependence on NC volume), (2) the PA amplitude steadily increases with photon energy with an onset greater than $2E_g$, and (3) it remains at low excitation fluences.

In addition to the TA experiments, MEG has been independently verified in the literature with two different PL measurements in CdSe[21] and InAs NCs.[11] Time-resolved photoluminescence (TRPL) single-photon-counting experiments measure both the dynamical signature of MEG, as in the TA experiments, as well as the biexciton PL spectrum under conditions where only one photon per NC is absorbed. Recently a quasi-CW measurement also observed the PL spectra of the multiexcitonic state in InAs[11] NCs under conditions where absorption of more than one photon per NC is very improbable. For Si NCs, TRPL measurements are extremely challenging due to the long single-exciton lifetimes (see Figure 1C) relative to typical TRPL laser repetition rates (50−250 kHz) and the large difference between biexciton and single lifetimes, which results in few photons being emitted within the biexciton lifetime. The quasi-CW method would also suffer from these limitations. TA measurements in Si NCs are complicated by the factor of ∼100 to ∼700 in the ratio of absorption cross sections for pump wavelengths below and above the MEG threshold. Hence we introduce a second method to acquire high-quality QY data with high SNRs that is a variation of the dynamical TA method described above. An additional benefit to this technique is that we can extract the absorption cross section at the pump wavelength, σ_p.

In this second method, we analyze the intensity dependence of the ratio of the exciton populations just after photoexcitation ($\tau \approx 0$) and after AR is complete ($\tau > 3t_2$), where τ is the pump−probe delay time and t_2 is the biexciton lifetime. Quantitative information regarding σ_p and quantum yield (QY) can be extracted using the following equation for R_{pop}, the ratio of populations at short ($\tau = t'$) and long delay ($\tau = t''$):

$$R_{pop} = \frac{\alpha_{photoinduced}(\tau = t')}{\alpha_{photoinduced}(\tau = t'')} = \frac{J_0 \cdot \sigma_p \cdot QY \cdot \delta}{1 - \exp(-J_0 \cdot \sigma_p)} \quad (3)$$

where $\alpha_{photoinduced}(\tau)$ gives the time-dependent PA signal, J_0 is the pump pulse photon fluence (photons·cm^{-2}·pulse^{-1}), and δ^{-1} is the single-exciton fractional decay occurring between delays of $\tau = t'$ and $\tau = t''$ (see Supporting Information for derivation of eq 3). Part A and B of Figure 4 present representative data sets for the 9.5 and 3.8 nm samples. The blue triangles are for photoexcitation above the MEG threshold, $3.3E_g$ and $2.9E_g$, and the red squares are for photoexcitation below the MEG threshold. Equation 3 is fit to each data set with only two adjustable parameters. For the sub-MEG threshold data, σ_p and δ are varied, while QY = 1.0. We find excellent agreement between our extracted σ_ps and those in the literature. For example, the 3.8 nm diameter sample yields a value of $\sigma_p(2.70 \text{ eV}) = 2.3 \times 10^{-16}$ cm^2, which compares well with absorption cross section measurements reported previously (∼2.0×10^{-16} cm^2) for this size of Si NC.[19] Our extracted cross sections also compare favorably with bulk absorption coefficients (see Figure 1A). For the above-MEG threshold, we hold fixed the value of δ determined for sub-MEG threshold excitation and vary the QY. We find for the 9.5 nm sample that, while the y-axis intercept is 1.5 when exciting below $2E_g$, the intercept of 2.9 for the case of $3.3E_g$ excitation indicates a QY of 1.9 ± 0.1, indicating very efficient MEG. The scatter in the data increases as the pump fluence decreases, as can be seen readily in Figure 4A. However, fitting the data set to eq 3 but excluding the lowest two points does not change the value of the QY significantly (within the fitting error). Hence the scatter at low fluence does not increase the uncertainty of our derived QY values. The best fit parameters have fitting errors of at most ∼10% (for the 3.8 nm sample) and only ∼5% for the 9.5 nm sample. Equation 3 is not strictly valid when the OD at the pump wavelength is large (OD > 1). One must account for the decreasing pump fluence as the pump light is absorbed in the sample. In this case, the extracted QY using eq 3 does not change; however, the extracted σ_p is underestimated. A complete simulation of this effect is possible because the OD at the pump wavelength is known. The values of σ_p that we report are for the low OD case where eq 3 is valid. For Figure 1, we scale the σ_p by the measured OD.

We have employed a combination of these two techniques to measure the MEG efficiency for a variety of pump wavelengths. The error bars in Figure 4C therefore represent the reproducibility of theses measurements. In general, fitting eq 3 to each individual data set resulted in fitting errors that were smaller than the reproducibility. While we can estimate from our data an onset of $2.5E_g$ for MEG, the precise value is obscured by the large-size dispersion of our samples.

Several theoretical models explaining the enhancement of MEG in quantum-confined NCs have been published, and disagreement remains.[8,12,22−24] The Bohr exciton radius (a_B) for Si is 4.9 nm, which is only slightly larger than half the 9.5 nm diameter Si NCs studied here. Because these 9.5 nm NCs are not in the weak confinement regime, defined as a
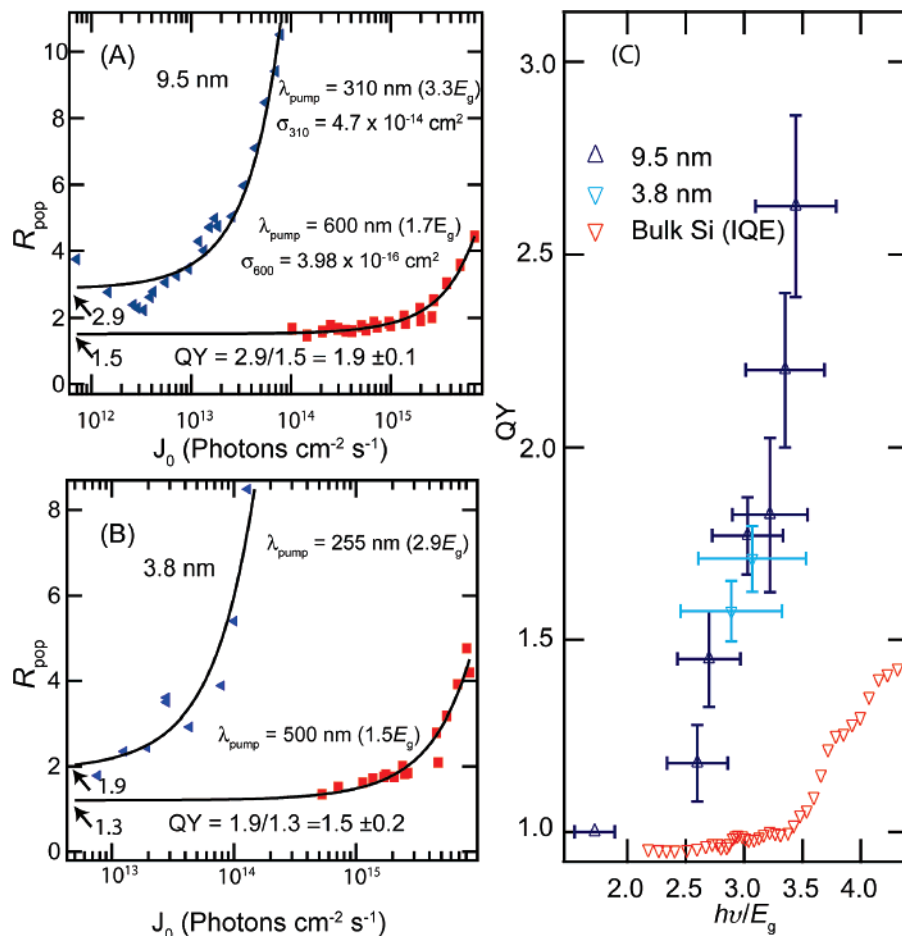
Figure 4. Ratio of the exciton populations at 3 and 1200 ps are plotted vs the pump photon fluence for (A) 9.5 nm sample and (B) 3.8 nm sample. The *y*-intercept represents the low-intensity limit of the ratio of the exciton populations initially after excitation (and prior to meaningful AR) to the population after multiexciton states have decayed to single-exciton states. (C) Compilation of all MEG QYs for the 9.5 (blue triangles) and 3.8 nm (light-blue triangles) samples. Red triangles are impact ionization quantum yields for bulk Si taken from ref 13.

> $\sim 3a_B$,[25] they are more appropriately characterized as being in the strong- to-intermediate regime despite the lack of a large spectral blue-shift. The present observation of efficient MEG in indirect-gap semiconductor NCs is an important result that has significance both for the theoretical model of MEG and for practical applications to solar photon conversion. This result implies that very strong confinement ($a_B \gg$ NC diameter), as evidenced by a large blue-shift of the band gap, is not necessary for efficient MEG, but only sufficient confinement is needed to produce stronger Coulomb coupling of the electrons and holes compared to the bulk, as discussed in ref 12. Other theoretical models for MEG would have to be consistent with this important feature.

On the practical side, the absence of the need for very strong confinement resulting in a large blue-shift of the band gap means that, for Si NCs, the band gap at which efficient MEG can occur lies close to the bulk band gap. Here, we find that 9.5 nm diameter Si NCs, with a band gap of 1.20 eV (only 80 meV larger than that of bulk bulk Si), show efficient MEG and that this band gap is close to the optimum NC band gap (0.9−1.1 eV) for the highest possible PV efficiency of 42% utilizing cells with MEG, yielding just 2 excitons per photon at a threshold of $2E_g$.[2] For an optimum

PV cell with 9.5 nm Si NCs, the maximum efficiency is already $\sim$41%, with two excitons/photon at the $2E_g$ threshold. However, to approach the highest possible PV efficiencies in actual solar cells, further research is needed to understand how to: (1) make the QY rise even more steeply with photon energy after the MEG threshold, (2) establish the threshold as close as possible to $2E_g$, and (3) dissociate the excitons into free, separated electrons and holes and collect them in an external circuit with a high efficiency. The latter process requires the time scale for exciton dissociation, charge transport, and separation to be fast compared to Auger recombination; to date, photocurrent measurements from NC structures show QYs < 1.0, indicating this has not yet been achieved.

Supporting Information Available: Intensity dependence of short- and long-delay PA signals for the 9.5 nm sample, TEM and size distribution of 9.5 nm Si NCs, derivation of eq 3. This material is available free of charge via the Internet at http://pubs.acs.org.

References

(1) Ross, R. T.; Nozik, A. J. *J. Appl. Phys.* **1982**, *53*, 3813.
(2) Hanna, M. C.; Nozik, A. J. *J. Appl. Phys.* **2006**, *100*, 074510/1−074510/8.
(3) Hybertsen, M. S. *Phys. Rev. Lett.* **1994**, *72*, 1514−1517.
(4) Iwamatsu, M. *Jpn. J. Appl. Phys., Part 1* **1998**, *37*, 5620−5621.
(5) Delerue, C.; Allan, G.; Reynaud, C.; Guillois, O.; Ledoux, G.; Huisken, F. *Phys. Rev. B* **2006**, *73*, 253318.
(6) Nozik, A. J. *Physica E* **2002**, *14*, 115−120.
(7) Schaller, R.; Klimov, V. *Phys. Rev. Lett.* **2004**, *92*, 186601.
(8) Ellingson, R. J.; Beard, M. C.; Johnson, J. C.; Yu, P.; Micic, O. I.; Nozik, A. J.; Shabaev, A.; Efros, A. L. *Nano Lett.* **2005**, *5*, 865.
(9) Schaller, R. D.; Petruska, M. A.; Klimov, V. I. *Appl. Phys. Lett.* **2005**, *87*, 253102.
(10) Murphy, J. E.; Beard, M. C.; Norman, A. G.; Ahrenkiel, S. P.; Johnson, J. C.; Yu, P.; Micic, O. I.; Ellingson, R. J.; Nozik, A. J. *J. Am. Chem. Soc.* **2006**, *128*, 3241−3247.
(11) Pijpers, J. J. H.; Hendry, E.; Milder, M. T. W.; Fanciulli, R.; Savolainen, J.; Herek, J. L.; Vanmaekelbergh, D.; Ruhman, S.; Mocatta, D.; Oron, D.; Aharoni, A.; Banin, U.; Bonn, M. *J. Phys. Chem C* **2007**, *111*, 4146−4152.
(12) Shabaev, A.; Efros, A. L.; Nozik, A. J. *Nano Lett.* **2006**, *6*, 2856−2863.
(13) Wolf, M.; Brendel, R.; Werner, J. H.; Queisser, H. J. *J. Appl. Phys.* **1998**, *83*, 4213.
(14) Mangolini, L.; Thimsen, E.; Kortshagen, U. *Nano Lett.* **2005**, *5*, 655−659.
(15) Green, M. A.; Keevers, M. *Prog. Photovoltaics* **1995**, *3*, 189−192.
(16) Credo, G. M.; Mason, M. D.; Burattoa, S. K. *Appl. Phys. Lett.* **1999**, *74*, 1978−1980.
(17) Jurbergs, D.; Rogojina, E.; Mangolini, L.; Kortshagen, U. *Appl. Phys. Lett.* **2006**, *88*, 233116.
(18) Wilson, W. L.; Szajowski, P. F.; Brus, L. E. *Science* **1993**, *262*, 1242.
(19) Kovalev, D.; Diener, J.; Heckler, H.; Polisski, G.; Kunzner, N.; Koch, F. *Phys. Rev. B* **2000**, *61*, 4485−4487.
(20) Klimov, V. I.; Mikhailovsky, A. A.; McBranch, D. W.; Leatherdale, C. A.; Bawendi, M. G. *Science* **2000**, *287*, 1011−1013.
(21) Schaller, R. D.; Sykora, M.; Jeong, S.; Klimov, V. I. *J. Phys. Chem B* **2006**, *110*, 25332−25338.
(22) Schaller, R. D.; Agranovitch, V. M.; Klimov, V. I. *Nat. Phys.* **2005**, *1*, 189.
(23) Franceschetti, A.; An, J. M.; Zunger, A. *Nano Lett.* **2006**, *6*, 2191−2195.
(24) Allan, G.; Delerue, C. *Phys. Rev. B* **2006**, *73*, 205423.
(25) Ekimov, A. J.; Hachre, F.; Schanne-Klein, M. C.; Richard, D.; Flytzanis, C.; Kudryavtsev, I. A.; Yazeva, T. V.; Rodina, A. V.; Efros, A. L. *J. Opt. Soc. Am. B* **1993**, *10*, 100.

NL071486L